Ocean Modelling 129 (2018) 1–12

Contents lists available at ScienceDirect

Ocean Modelling

journal homepage: www.elsevier.com/locate/ocemod

Modelling the mass exchange dynamics of oceanic surface and subsurface oil

Jorge Ramírez[a], Saeed Moghimi[b], Juan M. Restrepo[*,c], Shankar Venkataramani[d]

[a] Departamento de Matemáticas, Universidad de Colombia, Sede Medellín, Medellín, Colombia
[b] Department of Civil Engineering, Portland State University, Portland, OR, USA
[c] Department of Mathematics, Oregon State University, Corvallis OR, USA, Kavli Institute of Theoretical Physics, University of California Santa Barbara, Santa Barbara, CA, 93106, USA
[d] Mathematics Department, University of Arizona, Tucson, AZ 85721, USA

ARTICLE INFO

Keywords:
Oil spill
Oil fate model
Oil entrainment
Ocean oil transport
Ocean pollution

ABSTRACT

We propose a time dependent Eulerian model for sea surface entrainment, buoyancy transport and droplet dynamics of ocean oil. The model captures the microscale vertical oil mass exchanges in the neighborhood of the sea surface. This model is in turn part of an oil fate model designed to capture oil dynamics at large spatio-temporal scales typical of environmental studies. The adiabatic dynamics of the droplets are upscaled by a combination of filtering and stochastic parametrization. The upscaling addresses the computational burden of resolving the microscale. The upscaled droplet dynamics are tested against data and the mass exchange mechanism is incorporated into a nearshore oil transport model in order to highlight the importance of incorporating vertical mass exchanges and droplet distribution dynamics in predicting the distributing of shoaling oil.

1. Introduction

There are many ocean oil spill models (For reviews, see the ASCE Task Committee on Modeling of Oil Spills of the Water Resources Engineering Division, 1996 report and the Transportation Research Board and National Research Council, 2003 report. The latter of these reports has a good summary of the fundamental processes affecting oil spill dynamics in the ocean). OWN/OSCAR (from SINTEF), and SIMAP/OILMAP (from Applied Science Associates) are examples of commercial oil fate models. OWM (see Daling and Strom, 1999) is an oil weathering model. These packages include an oil-fate model along with a comprehensive suite of ancillary diagnostic/design modules useful in impact and planning assessments. Their oil transport models aim to be fairly comprehensive with regard to the inclusion of the many, and sometimes complex, mechanisms that alter the fate of oil in the ocean. Among non-commercial packages we could mention ADIOS (see Lehr et al., 1992; Lehr et al., 2002), and GNOME (see Zelenke et al., 2012), the NOAA Office of Response and Restoration model, along with MEDSLIK (see Dominicis et al., 2013) is the European Consortium model, and one of several European/Mediterranean model for surface oil spills. There are also a variety of oil plume models that are meant to capture blowouts and oil seeping from the ocean bottom. For example VOILS, described in Azevedo et al. (2014), and VDROP Zhao et al. (2014).

Most oil spill models are Lagrangian. Lagrangian oil fate models (see for example Lonin, 1999) are essentially parcel advection/diffusion schemes with added complex phenomenology. Many of these Lagrangian models import the wind and ocean velocity fields from separate ocean and wind circulation models. Eulerian models, similar to the one we are developing, are less common. Examples of Eulerian models are formulated in Tkalich and Chan (2002) (see also Tkalich and Chan, 2006), as well as in Wang and Shen (2010). Eulerian models are thought to be computationally less efficient (see Yapa et al., 1999) and this case may be made about some of them. An advantage of an Eulerian transport model is that, if properly designed, will be easily incorporated into an ocean circulation model. Further, if the circulation model has an optimized, high performance advection-diffusion solver, sophisticated grid generation capabilities, and time marching schemes, these can be used to great advantage in the efficient implementation and maintenance of the transport model/module. Compatibility in the boundary conditions and fluxes in the transport and the ocean circulation models are other important advantage. Presumably improvements in the (Eulerian) mixing and dispersion parameterizations in the ocean circulation can be exploited as well in improving the dynamics of the transport model.

The oil fate model we introduced in Restrepo et al. (2015) is Eulerian and is designed to be a tool in environmental work and thus is designed to capture oil spills at very large spatio-temporal scales, in

* Corresponding author.
E-mail address: restrepo@math.oregonstate.edu (J.M. Restrepo).

https://doi.org/10.1016/j.ocemod.2018.06.004
Received 28 September 2017; Received in revised form 22 June 2018; Accepted 26 June 2018
Available online 06 July 2018
1463-5003/

basins with very complex geometries and flows. Efficiency is paramount. Time spans from hundreds of seconds to seasons, and spatial scales spanning hundreds of meters to hundreds of kilometers. To reach these large spatio-temporal scales we have opted to pose the model in terms of depth-averaged equations. A consequence of depth-averaging is that the model will not capture the depth-dependence of the distribution of oil. The oil transport model is a *shallow-water* model, which means that it applies on problems where the variability of oil in the horizontal direction is much larger than the variability in the vertical direction. This does not imply that we ignore vertical variations in distribution of the oil within the water column that significantly affect the overall transport in transverse directions. It also makes no special requirements from the ocean code with regard to whether it resolves ocean vertical dynamics or not.

A depth-averaged model for oil dynamics makes geophysical sense in shallow waters. Specifically, in the shallow reaches of the continental shelf and large shallow lakes. Examples are the shelf areas, near the Gulf Coast states and the East Coast of the United States. The shelf is close to many major cities and sensitive habitats. The shelf zone has complicated shipping traffic, and a fair share of operational and dormant oil wells. Hence, the shelf is a zone of major environmental concern. These shallow oceanic regions have complex, topographically-dependent flows, complex coasts and river deltas. These conditions place enormous modeling challenges on sub-mesoscale ocean dynamics and small scale winds and coastal hydrodynamics. In many of these nearshore regions, upwelling is critical and thus the vertical dependence has to be explicit or carefully accounted for in the depth-averaging of the ocean flow simulations, not withstanding that we are going to ignore much of the vertical structure of the oil field.

In Restrepo et al. (2015) the general design of the oil fate model is laid out. In that same work the fundamentals of transverse oil advection and dispersion were worked out, as is the effect of the presence of oil on the dynamics of the ocean wave field. There are well-known challenges in developing a comprehensive oil model (and its computational platform) of the type we envision:

- Reaching the large spatio-temporal scales required by an environmental oil transport model will require a very large number of degrees of freedom, and by extension, of computational resources. In order to control the computational complexity of the resulting simulation platform it is necessary to design aspects of the physics and the computation simultaneously, thus allowing coupling of numerical resolutions and the physics in a consistent and efficient manner. The transport model we are building uses specialization to the shallow reaches of the continental shelf, where depth averaging and adiabatic assumptions apply, in order to reach high resolutions over large spatio-temporal expanses.
- A focus on the shallow reaches of the continental shelf requires coupling oil transport to nearshore dynamics, ocean dynamics at the submesoscale (see Romero et al., 2013; Uchiyama et al., 2014; Romero et al., 2016) as well as wind/weather fields and wave dynamics, the latter to capture wave-induced transport and dispersion (see McWilliams et al., 1997; McWilliams et al., 2004; Restrepo et al., 2011), and the former to generate the stresses on the ocean surface as well as on oil exposed to air. Coupling to a weather model would provide the requisite fields for an oil transport model that includes chemodynamics.
- The chemical composition of the oil, as a function of space and time, is important in a variety of environmental problems (see Thibodeaux, 1996). A model with the capacity to model chemodynamics would enable engineers the simulation capabilities to investigate weathering and dispersal via chemical means (see Li, 2009, Delvigne and Sweeney (1988), and Belore et al. (2009), and references contained in these for how dispersants affect oil). A long range goal of the modeling effort is thus to incorporate a comprehensive chemodynamics capability. Some chemical process, such as bio-degradation, sedimentation, and photolysis are already accounted for in mature oil models (see Lehr, 2001, Daling et al., 2014), and the documentation of ADIOS, GNOME, WON, SIMAP. Bio-degradation involves both the live population as well as the dead populations of many organisms. (See Loh et al., 2014). Chemodynamics would give an oil fate model the capability of making these processes reactive and dynamic.
  Chemistry also plays a role at microscopic scales: in the surface tension, buoyancy, viscosity of oil droplets. Changes in these in turn affect the oil droplet mechanics. Oil is a composite compound, consisting of hundreds if not thousands chemicals (see Thibodeaux, 1996; Hammam et al., 1988). Tracking these reacting chemicals adds significant complexity to the oil fate model. Moreover, the chemodynamics component adds a considerable computational burden to the resulting discretized oil fate model. Without some form of dimension reduction strategy the addition of chemodynamics can easily lead to an impractical oil transport model. Aggregation strategies, such as those used in combustion chemistry may prove helpful here (see Maas and Pope, 1992 and references contained therein. See also Daling et al. (2014) for an application of such strategies to oil spill models). Aggregation produces chemical complexes whose chemodynamics are seldom a linear superposition of their individual reactions. In Venkataramani et al. (2017) we developed a data-driven dimension reduction strategy that addresses non-standard behavior of chemical complexes. The strategy exploits Takens embedding in order to capture the memory terms that arise from the interaction of short-time and long-time dynamics. Unlike other strategies, our dimension reduction strategy leads to a reduction of computational degrees of freedom while at the same time reducing the inherent stiffness of the chemical complexes because it reduces the disparity of time scales. Thermodynamics and energy conservation enter chemical dynamics processes and can affect mass conservation as well. Mass conservation is a non-trivial and basic requirement in oil reservoir simulations, particularly in chemically-reacting flows (Chen, 2007), it is a complex problem in ocean oils. Examples include sedimentation rates (see Loebing, 2015), and the fact that oil gas near the sea surface can exist in liquid forms at depth and thus subjected to different dissolution dynamics (see Aman et al., 2015; Sokolofsky et al., 2011).
- Notwithstanding our interest in the macroscopic dynamics of the oil, the microscopic realm cannot be ignored (see Reed et al., 2009). The vertical transport is affected by droplet merging and splitting (merging and splitting is also affected by surface tension and viscosity which are thus dependent on the chemical dynamics). The mechanics of buoyancy, droplet dynamics, and turbulent processes near the ocean surface play important roles in the oil mass fluxes.

This study addresses the modeling challenges of the last item on this list, which we collectively call the *mass exchange dynamics*. Specifically, we want to formulate an upscaled dynamic model that captures oil entrainment by waves, the droplet merging/splitting dynamics, and Stokes force balances (buoyancy and drag) of distributions of droplets. The mass exchange refers to capturing the exchanges of oil between the surface and subsurface components of the oil fate model. We will not account for chemistry at this stage.

Most models for oil transport take into account oil mass exchanges between surface and the subsurface. The SINTEF products (see Reed et al., 2009), for example, will use a combination of empirically-derived and mechanical models based mainly on equilibrium conditions for this exchange. We will include mechanics of droplet merging and splitting, along the lines proposed in Tsouris and Tavlarides (1994). The micromechanics of buoyancy/drag and of surface mixing due to wave breaking extend the model suggested in Tkalich and Chan (2002) to include a parametrization of wave breaking based on results found in Restrepo et al. (2011). Hereon, Tkalich and Chan (2002) will be denoted as TC). Using upscaling/filtering, the resulting non-stationary

model will approximately capture micromechanics without resolving these. It can thus be incorporated into an Eulerian oil transport model, such as the one proposed in Restrepo et al. (2015).

This paper is organized as follows: in Section 2 we briefly summarize the shallow-water oil model and identify where the mass exchange term appears in the transport equation. The full details on the advection and diffusion/dispersion in the transport equations can be found in Restrepo et al. (2015). The mass exchange mechanism between surface and subsurface oil is proposed in Section 3, as well as the evolution of the droplet size distribution and merging/splitting dynamics. The upscaling strategy of the vertical oil exchanges is described in Section 4. In Section 5 we compare the reduced-dimension droplet distribution model to data, and by extension, to another droplet model. In Restrepo et al. (2014) we proposed a model for the slowing down and possibly parking of buoyant pollutants and tracers in oceanic regions adjacent and offshore of the break zone. The term 'nearshore sticky waters' is used to describe the conditions that lead to slowing/parking of incoming pollutants. The 'stickiness' is a result of the advective and dispersive conditions near the break zone and the conditions whereby the effective transport velocity decreases or goes to zero, away from the shore, depends in turn on the vertical distribution of the buoyant pollutant. In Restrepo et al. (2014) we prescribed the vertical distribution. In Section 5 of this study we revisit the nearshore sticky water problem and replace a prescribed vertical distribution by one given dynamically by the mass exchange model developed here. We confirm that sticky water conditions are still possible and show how the droplet distribution has a bearing on how the transport unfolds. In Section 6 we summarize the model and its features.

2. The shallow-water oil fate model

The framework of the oil fate model appears in Restrepo et al. (2015). The general transport model is formulated for a surface slick layer S, in units of length that represents the effective thickness of surface oil, and a subsurface component of oil, described by a concentration field C in units of density times volume over volume. There may be hundreds to thousands of chemicals in a any sample of oil and each oil spill may have different chemical composition. We take this into account and describe the slick as a composite of homogeneous sub-slicks, each of thickness s_i. Hence,

$$S(\mathbf{x},\, t) \;= \sum_{i=1}^{N} s_i(\mathbf{x},\, t), \tag{1}$$

where N is the total number of chemical complexes. The total oil slick mass is then given by

$$M_s(T) = \int_{\Omega_T} \sum_{i=1}^{N} s_i(\mathbf{x},\, T)\rho_i d\mathbf{x}, \tag{2}$$

where $\mathbf{x}$ is the transverse coordinate, Ω_T is the (possibly time dependent) oceanic domain or area of interest. Time is denoted by T, and is understood as associated with the time scales in which advection/diffusion/dissipation takes place (as opposed to the shorter time scales of the micromechanics). The densities of each chemical complex are denoted by the ρ_i.

For the *ith* chemical complex, the transport equation is

$$\frac{\partial s_i}{\partial T} + \nabla_\perp\cdot\left(C_{xs}\mathbf{V}s_i + \frac{\boldsymbol{\tau}}{2\mu_i}s_i^2\right) - \nabla_\perp\cdot[\Psi\nabla_\perp s_i] = R_i + E_i^s(s_i) + P_i^s + G_i^s. \tag{3}$$

Here, $\nabla_\perp$ is the transverse gradient operator, $\mathbf{V}$ are the $\mathbf{x}$-components of the transport velocity, C_{xs} is a slip parameter, $\boldsymbol{\tau}$ is the wind stress, μ_i the viscosity of the *ith* oil species. The last term on the left hand side is the eddy dispersion term with Ψ denoting its rate tensor (its symmetric component is associated with diffusion and the antisymmetric part with advection). R_i is the rate associated with mass exchanges between the oil slick and the interior of the ocean and is the focus of this study. The reaction term $E_i^s(b_i, s_i, s_j)$ encompasses chemical reactions among chemical complexes within the slick as well as other processes modeled by rates, such as evaporation. P_i^s is the rate of biodegradation, emulsification, photodegradation and G_i^s is the source rate term. Unlike R_i the terms with s superscript are particular to the surface oil.

The total mass of the oil in the sub-surface is defined as

$$M_c = \int_{\Omega_T}\int_{-h}^{\eta}\sum_{i=1}^{N} c_i(\mathbf{x},\, z,\, T)\, dz\, d\mathbf{x}. \tag{4}$$

where c_i is the concentration of the *ith* chemical complex in the subsurface layer, in units of M/L^3. We define the depth averaged subsurface concentration of the *ith* complex as

$$C_i(\mathbf{x},\, T) := \frac{1}{H(\mathbf{x})}\int_{-h}^{\eta(T)} c_i(\mathbf{x},\, z,\, T)\, dz, \tag{5}$$

where H is the total water column depth. Note that the product HC_i has units of M/L^2 and its evolution is given by

$$\frac{\partial HC_i}{\partial T} + \nabla_\perp\cdot(H\mathbf{V}C_i) - \nabla_\perp\cdot[H\Psi\nabla_\perp C_i] = -\rho_i R_i + \rho_i[E_i^C(C_i) + P_i^C + G_i^C]. \tag{6}$$

On the right hand side, the first term is the mass exchange term $\rho_i R_i$, the reaction/chemistry term is E_i^C, P_i^C represents the sedimentation and biodegradation mechanisms. The subsurface source term is G_i^C. This paper concerns itself with developing a model for R_i, which is related to the mass exchange term, and it has units of L/T.

3. The mass exchange model

The term R represents oil gained by the slick from the subsurface by buoyancy and lost by mixing and wave breaking (for an alternative model, see Reed et al., 2009). Because buoyancy forces depend on the radius of the droplets, it is necessary to keep track of the droplet distribution in the subsurface, which in turn, requires that droplet merging and splitting be incorporated in the dynamics. The consequence of this is that micromechanics need to be resolved or they must be upscaled if the scales of interest are far larger than the droplet coherence scale. Here, as in Restrepo et al. (2015), we develop the rationale for an upscaled version of the mass exchange process to environmental spatio-temporal scales.

3.1. Slick/subsurface oil exchanges

Focusing on the ith chemical species, and making use of M_s and M_c from (2) and (4) respectively, gives the total mass per unit area of oil at a fixed transverse location $\mathbf{x}$ and time T as

$$m_i(\mathbf{x},\, T) \;= H(\mathbf{x})C_i(\mathbf{x},\, T) + \rho_i s_i(\mathbf{x},\, T) \tag{7}$$

$$= \int_{-h}^{\eta(T)} c_i(\mathbf{x},\, z,\, T)\, dz + \rho_i s_i(\mathbf{x},\, T)$$

$$= \int_{-h}^{\eta(T)}\int_0^{\infty} \rho_i V(r) n_i(\mathbf{x},\, z,\, r,\, T)\, dr\, dz + \rho_i s_i(\mathbf{x},\, T). \tag{8}$$

The last term in (8) represents the slick contribution, the first term on the right of (8) represents the submerged oil in terms of droplets of radii r and volume $V(r) = \frac{4}{3}\pi r^3$ and their space-time varying distribution $n_i(\mathbf{x}, z, r, t)$. The dynamics model for n_i will be developed in Section 3.3. $n_i(\mathbf{x}, z, r, t)\, dr$ gives the number of droplets of radii in $(r, r + dr)$ per unit volume of water and at depth z. Hence, n_i has units of L^{-4}.

In order to describe the dynamics of the submerged portion of the ith chemical complex c_i and HC_i in (5) and (6), one must account for the fraction occupied by such chemical complex within each of the submerged droplets. Consider the total mass of such chemical stored in droplets submerged in the volume of water $d\mathbf{x}dz$: there are $n_i\, d\mathbf{x}\, dz\, dr$ of them with radii in $(r, r + dr)$, and we may assume that the jth droplet

contains a random fraction $F_{i,\,j}$ of the *ith* chemical within it. We hence approximate:

$$c_i\,d\,\mathbf{x}\,dz \;= \mathbb{E}\int_0^\infty \rho_i V(r) \sum_{j=1}^{n\,d\mathbf{x}\,dz\,dr} F_{i,j}(z,\,r) = \int_0^\infty \rho_i V(r)\overline{F_i}(z,\,r)n(\mathbf{x},\,z,\,r,\,t)dr\,d\mathbf{x}\,dz, \tag{9}$$

with $\overline{F_i}(r,\,z)$ denoting the average fraction of chemical i contained in droplets of radius r submerged at depth z.

The total amount of chemical complex i per unit area in the water column can therefore be written as

$$m_i(\mathbf{x},\,T) = \int_{-h}^{\eta(T)}\int_0^\infty \rho_i V(r)n(\mathbf{x},\,z,\,r,\,T)\overline{F_i}(z,\,r)\,dr\,dz + \rho_i s_i(\mathbf{x},\,T). \tag{10}$$

If we ignore the dispersion, wind forcing, reaction/chemistry, sedimentation, biodegradation and subsurface sources, the total derivatives of m_i in (7) and m_i given by (10) must be consistent. Therefore

$$\frac{\partial HC_i}{\partial T} + \mathbf{V}\cdot\nabla(HC_i) + \rho_i R_i = -\rho_i\left[\frac{\partial s_i}{\partial T} + \mathbf{V}\cdot\nabla s_i - R_i\right], \tag{11}$$

where R_i is the exchange term (see (3) and (6)) and may be conveniently decomposed as:

$$R_i = R_i^{\uparrow} - R_i^{\downarrow} = \int_0^\infty V(r)w_b(r)n_i(\mathbf{x},\,\eta,\,r,\,T)\,dr - s_i(\mathbf{x},\,T)b(\mathbf{x},\,T). \tag{12}$$

The component $R_i^{\uparrow}$ is the rate of oil gained by the slick (in units of length/time) coming from the subsurface by means of buoyancy, with $w_b \geq 0$ denoting the upwards velocity of the buoyant droplets oil, which is here supposed to depend only on their radius as any effects of internal droplet composition have been averaged out. The second term $R_i^{\downarrow} = s_i b$ is the rate of oil lost from the slick due to wave breaking and will be described in Section 3.2 below (also see TC for an alternative derivation).

Disregarding all processes of chemical degradation and exchange, the quantities HC_i and s_i satisfy an equation identical to (11) but involving the corresponding mass exchange rate R_i which may also be decomposed as $R_i = R_i^{\uparrow} - R_i^{\downarrow}$, where

$$R_i^{\uparrow} = \int_0^\infty V(r)w_b(r)\overline{F_i}(r,\,\eta)n(\mathbf{x},\,\eta,\,r,\,T)\,dr. \tag{13}$$

3.2. The wave breaking term $R_i^{\downarrow}$

Wave breaking occurs within the location $\mathbf{x}$ and $\mathbf{x} + d\mathbf{x}$ at a rate of λ_b events per unit time, each having a 'strength' that may be characterized in terms of the wave slope ka, where k is the wavenumber and a is the wave amplitude, of the breaking wave (see Restrepo et al., 2011). For the time scales of interest, a wave breaking event occurring at time T_k can be regarded as an instantaneous transport event in which a fraction b_k of the available volume $S(\mathbf{x},\,T_k)d\mathbf{x}$ is injected and distributed into the water column. Let $\delta_{T_k}(T)$ denote the delta function at time T_k, namely $\delta_{T_k}(T) = \frac{1}{dT}$ for $T \in [T_k,\,T_k + dT)$, and zero everywhere else. The breaking inputs can then be written in terms of a compound Poisson N_b process of rate λ_b yielding the following expression for b in (12):

$$b(\mathbf{x},\,T) = \sum_{i=1}^{N_b(T)} b_k\delta_{T_k}(T). \tag{14}$$

We will refer to the unitless b_k as the *strength* of the *kth* wave breaking event. Note that the units of b are 1/T.

Droplets created from the available volume $S(\mathbf{x},\,T)b(\mathbf{x},\,T)d\mathbf{x}$ are the source term for the equation describing the dynamics of n which is derived in Section 3.3 below. Hence, we now decompose Sb into the appropriate distributions of radii and depths. According to Delvigne and Sweeny (1988), if a unit of oil per unit area is available to be distributed into droplets, the number of droplets per unit volume of oil and of radius in $(r,\,r + dr)$ will be $N(r)\,dr$, with

$$N(r) := \frac{3(4-s^*)}{4\pi(r_m^{4-s^*} - r_1^{4-s^*})}r^{-s^*},\;\; r \in [r_1,\,r_m],\quad s^* \neq 3, \tag{15}$$

zero otherwise, which is such that $\int_0^\infty V(r)N(r)\,dr = 1$. The units of N are L^{-4}, the empirical parameter s^* is frequently quoted as taking the value of 2.3 (see TC). The resulting droplets are distributed along the water column according to a function $g_b(z)$ which we assume does not depend on anything besides z, and satisfies

$$\int_0^\infty g_b(z)\,dz = 1. \tag{16}$$

The distribution of droplet sizes (15), proposed by Delvigne and Sweeny, is not universally accepted. For example, Reed et al. (2009) propose a log-normal fit to droplet distributions instead, based upon laboratory data. (See Mitzenmacher, 2003 for a discussion on the challenges associated with fitting certain types of data to log-normal and power law distributions).

The density of available droplets of radius r at depth z, per unit area, is denoted

$$S_b(\mathbf{x},\,z,\,r,\,T) = N(r)g_b(z)b(\mathbf{x},\,T)S(\mathbf{x},\,T) \tag{17}$$

which has units of $\mathrm{T}^{-1}\mathrm{L}^{-4}$ and, by virtue of (1), (15) and (16), satisfies

$$\int_{-h}^{\eta}\int_0^\infty V(r)S_b(\mathbf{x},\,z,\,r,\,T)dr\,dz = b(\mathbf{x},\,T)S(\mathbf{x},\,T) =: R^{\downarrow}. \tag{18}$$

As for the mass transport $R_i^{\downarrow}$ of the ith chemical from the slick into the water column, we assume that wave breaking acts indiscriminately on the composite slick, and that the following balance holds

$$R_i^{\downarrow} = \frac{s_i}{S}R^{\downarrow}. \tag{19}$$

3.3. Subsurface droplet distribution dynamics

We must now specify a dynamic model for the droplets in the subsurface that includes S_b in (17) as a source term. In accordance with the oil model (Restrepo et al., 2015), droplets are assumed to undergo a linear vertical advection-diffusion process. Furthermore, the time scales at which the vertical distribution of oil sorts itself out, given fast disturbances at the sea surface, are assumed to be very short compared to the horizontal advection scales (the shallow water wave approximation).

We denote the vertical turbulent diffusivity by $D_z(r) \sim 10^{-2}$-$10^{-3}\mathrm{ms}^{-2}$ which can be parametrized in terms of the turbulent description of the flow, while $w_b(r) \sim 10^{-6}$-10^{-3-1} is the limiting velocity of a oil droplet moving through water. The values ranges for D_z and w_b are taken from TC, Eq. (13).

In what follows we focus on vertical balances, an adiabatic approximation, in which for given radius r, depth z and time T, two flux sources affect $n(\mathbf{x},\,z,\,r,\,t)$: the droplets that are entrapped from the surface into depth z after a wave breaking event, and changes on the distribution of radii due to merging and splitting of droplets. Putting all together, gives

$$\frac{\partial n}{\partial T} = D_z(r)\frac{\partial^2 n}{\partial z^2} - (W(\mathbf{x},\,z,\,T) + w_b(r))\frac{\partial n}{\partial z} + S_b + \mathcal{K}[n], \tag{20}$$

Furthermore, the background vertical velocity satisfies $W \ll w_b(r)$ and will hence be ignored. The operator $\mathcal{K}$ encodes the effect of merging and splitting of droplets. This operator is discussed in detail in Section 4.1, but for now, it suffices to remark that it should be conservative, namely

$$\int_0^\infty \mathcal{K}[n](r)\,dr = 0. \tag{21}$$

At the surface $z = \eta(T)$ we assume that there is no diffusive flux as

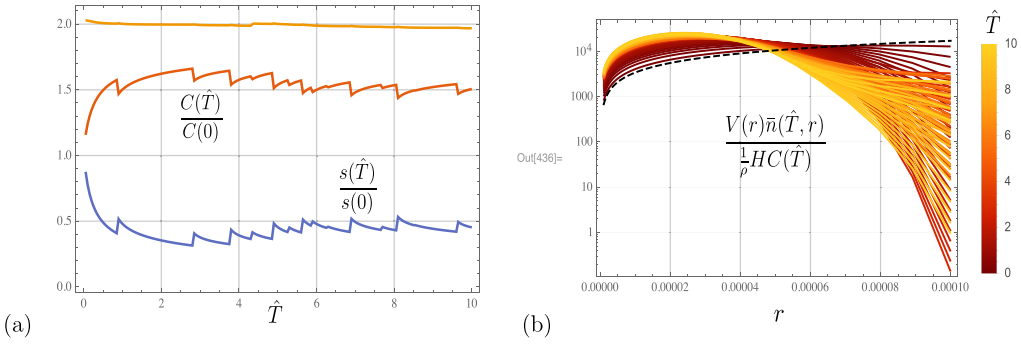

Fig. 1. (a) Evolution of non-dimensional surface $s/s(0)$ (lower) and subsurface oil $C/C(0)$ (mid), and their sum (upper): $s(0)$ and $C(0)$ are initial surface and subsurface concentrations. The sharp changes coincide with the breaking events. Mass is conserved to within acceptable numerical accuracy. (b) Time evolution of the fraction of volume of subsurface entrapped oil, as a function of time and radii. Initially the distribution of droplet sizes had a greater number of larger droplet sizes (dashed). The various curves correspond to different times. The fraction of small droplets steadily increases with time.

the slick is saturated, while all incoming droplets from the upward effect of buoyancy are added to s and removed from the concentration n. The boundary condition at the subsurface/slick interface is simply:

$$\frac{\partial n}{\partial z}(t,\eta,r)=0,\quad t>0,\ r\in[0,\infty). \tag{22}$$

At $z=-h$ we allow for sedimentation, which we ignore for now.

In what follows we fix $\mathbf{x}$ (which we omit in the subsequent notation), and solve for the amount of oil in the slick and subsurface droplets occupying the one-dimensional moving water column $(-h,\eta(T))$, ignoring as well horizontal advection/dispersion. Specifically, we solve

$$\frac{\partial n}{\partial T}=D_z(r)\frac{\partial^2 n}{\partial z^2}-w_b(r)\frac{\partial n}{\partial z}+S_b(z,r,T)+\mathcal{K}[n] \tag{23}$$

$$\frac{\partial s}{\partial T}=\int_0^\infty V(r)w_b(r)n(r,\mathbf{x},\eta,T)\,dr-s(T)b(T). \tag{24}$$

The first term on the right hand side of (23) represents, effectively, stochastic diffusion in the z direction and could be equivalently written in terms of stochastic Wiener process for the movement of individual droplets.

The solution to (23) is:

$$\begin{aligned}n(r,z,T)&=\int_0^T\int_{-h}^{\eta(T')}G(r,z',z,T-T')(\mathcal{K}[n]+\mathcal{S}_b)(r,z',\mathcal{T}')\,dz'\,d\mathcal{T}'\\&=\sum_{k=0}^{N_b(T)}\int_{-h}^{\eta(T_i)}g_b(z')G(r,z',z,T-T_i)\,dz'\,N(r)s(T_k)b_k\\&\quad+\int_0^T\int_{-h}^{\eta(T')}G(r,z',z,T-T')\mathcal{K}[n(\cdot,z',\mathcal{T}')](r)\,dz'\,d\mathcal{T}'\end{aligned} \tag{25}$$

where we have made the convenient choice for the initial condition

$$n(0,z,r)=\frac{1}{\rho}HC(0)N(r)g_b(z) \tag{26}$$

and set $T_0=0$, $b_0=\frac{\frac{1}{\rho}HC(0)}{s(0)}$. The function G in (25) is the Green's function associated with the parabolic Eq. (20) of n which may be approximated with the Green's function corresponding to the operator $w_b\partial_z+D_z\partial_z^2$ on $(-\infty,\eta)$, with boundary condition (22). That is to say,

$$\begin{aligned}G(r,z,z',T)&=\frac{1}{2\sqrt{\pi TD_z}}\left\{\exp\left[-\frac{(z'-z)^2}{4TD_z}\right]+\exp\left[-\frac{(2\eta-(z+z'))^2}{4TD_z}\right]\right\}\\&\quad\times\exp\left[-\frac{w_b(2(z'-z)+Tw_b)}{4D_z}\right]\\&\quad-\frac{1}{2D_z}w_b\exp\left[\frac{(\eta-z')w_b}{D_z}\right]\operatorname{erfc}\left[\frac{2\eta-(z+z')+Tw_b}{2\sqrt{TD_z}}\right].\end{aligned} \tag{27}$$

As an illustration, we consider first the simplest of possible situations: the dynamics of the mass exchange and its impact on the slick and subsurface oil supposing $\mathcal{K}\equiv 0$. The following simple backwards difference scheme is used for the approximate solution of s

$$s(T)\approx\frac{s(T-\Delta T)+\Delta T\,R^{\uparrow}(T)}{1+\Delta T\,b(T)}$$

where the mass transport into the slick can be written as

$$\begin{aligned}R^{\uparrow}(T)=\sum_{i=0}^{N_b(T)}s(T_i)b_i\delta_{T_i}(T)\int_0^\infty V(r)w_b(r)N(r)\int_0^\infty g_b(z')G(T\\-T_i,z',0,r)\,dz'\,dr.\end{aligned}$$

For this illustrative example, we use the parametrization of $w(r)$ and $D(r)$, suggested by TC, $w(r)=\frac{2g(1-\rho/\rho_w)}{9\nu_w}r^2$, $D(r)=D_0\left(\frac{D_0}{D_m}\right)^{-\frac{r}{r_m}}$, with $\rho=800\text{kg m}^{-3}$, $D_0=10^{-2}\text{m s}^{-1}$, $D_m=10^{-3-1}$, $r_1=10^{-6}\text{m}$, $r_m=10^{-4}\text{m}$ (1, 100 μm, respectively). The rate of breaking was set as $\lambda_b=10^{-3-1}$ and the fraction of entrapped oil randomly distributed as $b_i\sim\text{Uniform}(0,10^{-1})$. After a breaking event, the entrapped volume is distributed exponentially over the depth so 95% of it is above $z_m=1\text{m}$, $g_b(z)=\kappa e^{-\kappa z}$ with $\kappa=3\text{ m}^{-1}$.Fig. 1a describes the evolution of the fraction of slick and subsurface oil, as a function of time. The breaking events are clearly evident in the curves. The upper curve in Fig. 1a is the total mass, the middle is the normalized subsurface concentration and the lower curve the surface oil depth. In Fig. 1b we plot the fraction of volume of entrained oil, as a function of radii, for several times (see (28) for the definition of $\bar{n}$). The dashed curve is the original distribution. The distribution shifts toward the smaller radii with time. Non-dimensional quantities are computed with respect to the reference values D_m, z_m: $\widehat{T}=\frac{D_m}{z_m^2}T$, $\widehat{w_b}=\frac{z_m}{D_m}w_b$, $\widehat{D}=\frac{D}{D_m}$, $\widehat{\lambda}_b=\frac{z_m^2}{D_m}\lambda_b$.

4. Upscaled dynamics

When the oil spill is young, or the sea state is rough, droplet distributions change quickly due to merging and splitting. Further, it is often assumed that droplets in the subsurface smaller than a critical radius, will remain in the subsurface (see TC and references contained therein for the basis for such an assumption. See also Reed et al. (2009)). The critical radius for ocean oil is quoted in TC as $r_c=50\mu\text{m}$. For computational reasons it is convenient to bin droplet sizes for each chemical complex and formulate the subsurface oil transport in terms of a finite, discrete set of droplet classes. At the same time, we incorporate depth-averaging and pose the dynamics of subsurface droplets in terms of fluxes into and out of the depth-averaged horizontal computational cells due to advection/dispersion, interactions with the slick via buoyancy and wave mixing, and finally via changes to droplet class distributions within each cell.

We now use (23)–(24) to obtain a set of equations for the number of total droplets per unit area of ocean in prescribed radii classes. Namely, let $r_1<r_2<\cdots<r_m$ be a subdivision of radii of interest into m classes and $\Delta r=r_{j+1}-r_j$. We are interested in the evolution of

$$\bar{n}_j(\mathbf{x},T)=\int_{-h}^{\eta}\int_{r_j}^{r_{j+1}}n(\mathbf{x},z,r,T)\,dr\,dz. \tag{28}$$

Invoking (25), it can be written as (omitting the $\mathbf{x}$-dependence)

$$\overline{n}_j(T) = \sum_{k=0}^{N_b(T)} \widehat{G}_j(T - T_k)s(T_k)b_k + \int_{r_j}^{r_{j+1}}\int_0^T\int_{-h}^{\eta(T)}\int_{-h}^{\eta(T')} G(r, z', z, T - T')\mathcal{K}[n(\cdot,z', \mathcal{T}')](r)\,dz'\,dz\,d\mathcal{T}'\,dr, \tag{29}$$

where,

$$\widehat{G}_j(T) = \int_{r_j}^{r_{j+1}}\int_{-h}^{\eta(T)}\int_{-h}^{\eta(T')} G(r, z', z, T)g_b(z')N(r)\,dz'\,dz\,dr. \tag{30}$$

We would like to derive an expression for the dynamics of merging and splitting of droplets that is independent of z and hence arrive to an approximate version of (29) in terms of solely $\overline{n}_j$. We may assume that the merging and breaking processes occur at time scales much shorter than those of T. In particular, during an interval dT', the change in the distribution of radii is

$$n(r, z', T' + dT') - n(r, z', T') \approx \mathcal{K}[n(\cdot,z', \mathcal{T}')]d\mathcal{T}'. \tag{31}$$

Out of these added droplets, the following amount is then transported to depth z

$$\int_{-h}^{\eta(T')} G(r, z', z, T - T')\mathcal{K}[n(\cdot,z', \mathcal{T}')](r)d\mathcal{T}'\,dz'. \tag{32}$$

We approximate the second integral in (29) by commuting these mechanisms, thus obtaining

$$\int_0^T\int_{-h}^{\eta(T)}\int_{-h}^{\eta(T')} G(r, z', z, T - T')\mathcal{K}[n(\cdot,z', \mathcal{T}')]\,dz'\,dz\,d\mathcal{T}' \approx \int_0^T \mathcal{K}\left[\int_{-h}^{\eta(\mathcal{T})}\int_{-h}^{\eta(\mathcal{T}')} \mathcal{G}(\cdot,z', z, \mathcal{T} - \mathcal{T}')n(\cdot,z', \mathcal{T}')\,dz'\,dz\right]d\mathcal{T}' \tag{33}$$

which essentially disregards the depth-wise structure of n when it comes to the merging and splitting mechanism. Note that for every r,

$$u(r, z, T, T'): = \int_{-h}^{\eta(T')} G(r, z', z, T - T')\,n(r, z', T')\,dz'$$

is a solution to the problem $\partial_T u = -w_b\partial_z u + D_z\partial_z^2 u$ on $(-\infty, \eta)$, $T > T'$, with boundary conditions $u_z(\eta, T) = 0$ and initial condition $u(r, z, T', T') = n(z, r, T')$. The depth integral of u satisfies

$$\frac{\partial}{\partial T}\int_{-h}^{\eta(T)} u(r, z, T, T')dz = -w_b u(r, \eta, T'T) \approx -\frac{w_b}{H}\int_{-h}^{\eta(T)} u(r, z, T, T')dz$$

for $T > T'$. Namely,

$$\int_{-h}^{\eta(T)} u(r, z, T, T')dz \approx \int_{-h}^{\eta(T)} n(r, z, T')dz\; e^{-\frac{w_b}{H}(T-T')}$$

The integral in the last expression is the depth-integrated size distribution of droplets,

$$\overline{n}(r, T') = \int_{-h}^{\eta(T')} n(r, z, T')\,dz \tag{34}$$

Eq. (29) therefore simplifies and we approximately obtain an equation in terms of only depth-averaged size distributions:

$$\overline{n}_j(T) \approx \sum_{k=0}^{N_b(T)} \widehat{G}_j(T - T_k)s(T_k)b_k + \int_{r_j}^{r_{j+1}}\int_0^T e^{-Hw_b(r)(T-T')}\mathcal{K}[\overline{n}(\cdot,\mathcal{T}')](r)\,d\mathcal{T}'\,dr \approx \sum_{k=0}^{N_b(T)} \widehat{G}_j(T - T_k)s(T_k)b_k + \int_0^T e^{-Hw_b(r_j)(T-T')}\mathcal{K}[\overline{n}(\cdot,\mathcal{T}')](r_j)\,d\mathcal{T}'. \tag{35}$$

To recover the sub-surface concentration of the ith chemical, we take another average over the fraction of chemical F_i contained in each droplet. Let

$$\overline{\overline{F}}_{i,j}: = \frac{1}{H}\int_{-h}^{\eta} \overline{F}_i(r_j, z)dz. \tag{36}$$

Using (5) and (9), and the approximations $V(r) \approx V(r_j)$, and $\overline{F}_i(z, r) \approx \overline{F}_i(z, r_j)$ for $r \in (r_j, r_{j+1})$ and $\overline{F}_i(z, r_j) \approx \overline{\overline{F}}_{i,j}$ we obtain

$$C_i = \frac{1}{H}\sum_{j=1}^{m} \rho_i V(r_j)\overline{n}_j\overline{\overline{F}}_{i,j}. \tag{37}$$

In arriving at (37) we also used the approximation $F_i(r_j, \eta)n(r_j, x, \eta, T) \approx F_i(r_j, \eta)\overline{n}_j$.

By integrating of (24), and focusing attention on the ith complex, we arrive at the following corresponding upscaled equation for the slick oil

$$\frac{\partial s_i}{\partial T} = \sum_{j=1}^{m} \frac{V(r_j)w_b(r_j)}{H}\overline{F}_i(r_j, \eta)\overline{n}_j - \sum_{k=0}^{N_b(T)} s_i(T_k)b_k\delta_{T_k}(T). \tag{38}$$

The chemistry dynamics equations are necessary to determine the ultimate relation between $\overline{F}_i(r_j, \eta)$ at the surface and the depth-integrated $\overline{\overline{F}}_{i,j}$. The chemodynamics is an aspect of the shallow-water oil transport model that is yet to be developed.

4.1. Subsurface oil droplet merging and coalescence

We will focus now on the droplet merging/splitting mechanism, captured by the operator $\mathcal{K}$. We consider the situation for a subsurface cell at position $\mathbf{x}$. In what follows we dispense tagging the variables with their chemical species and ignore other mechanisms that affect the distribution of droplets in a compartment or cell. The total number of droplets of size class in $(V(r), V(r + dr))$ occupying the volume of water under $d\mathbf{x}$ is $\overline{n}$ defined in (35), which changes due to breaking and merging as

$$\mathcal{K}[\overline{n}] = (\mathcal{B}_V - \mathcal{D}_V), \tag{39}$$

where D_V, B_V are death and birth rates that approximate the Smoluchowsky operator $\mathcal{K}$. The death D_V and birth B_V terms, in turn, are defined as

$$D_V = \overline{n}(V, T)\int_0^\infty \lambda(V, V')h(V, V')\overline{n}(V', T)dV' + g(V)\overline{n}(V, T), \tag{40}$$

$$B_V = \int_0^{\frac{V}{2}} \lambda(V - V', V')h(V - V', V')\overline{n}(V - V', T)\overline{n}(V', T)dV' \tag{41}$$

$$+ \int_V^\infty \beta(V, V')\nu(V')g(V')\overline{n}(V', T)dV', \tag{42}$$

where $V \coloneqq V(r)$, $V' \coloneqq V(r')$. In the above expressions $\lambda(V, V')$ is the coalescence efficiency for collisions between droplets of classes V and V', $h(V, V')$ is the frequency of droplets of class V colliding with droplets of class V', $g(V')$ is the breakage frequency of droplets of class V', $\nu(V')$ represents the number of droplets formed by the splitting of droplets of class V' and $\beta(V, V')$ is the probability of forming droplets of class V from splitting of droplets of class V'. To first order, it can be assumed that only binary collisions occur, and thus $\nu(V') = 2$.

Once the droplet distribution is binned (assuming the total number of bins m is even), the $HD_j(\cdot,T) \approx D_{V(r_j)}$ and $HB_j(\cdot,T) \approx B_{V(r_j)}$ are:

$$HD_j = \overline{n}_j(T)\sum_{l=1}^{m} \lambda(r_j, \eta)h(r_j, \eta)\overline{n}_l(T) + g(r_j)\overline{n}_j(T), \tag{43}$$

$$HB_j = \sum_{l=1}^{m/2} \lambda(r_j - r_l, \eta_l)h(r_j - \eta_l, \eta_l)\overline{n}(r_j - r_l, T)\overline{n}_l(,T) + \sum_{l=j}^{m} 2\beta(r_j, \eta_l)g(\eta_l)\overline{n}_l(,T). \tag{44}$$

4.1.1. Parametrizing breakup mechanics

Droplet breakup is caused when an external force in the surrounding fluid exceeds the surface and internal forces in the droplet (see Liao and Lucas, 2009). Specific breakup mechanisms are: droplet elongation in sheared flow, turbulent pressure fluctuations, relative velocity fluctuations, and droplet-eddy collisions. (The large eddies will advect droplets, but those turbulent eddies that are comparable in size or smaller will exert a shear when they interact with a droplet of oil). The breakup frequency, f, assuming droplet-eddy collisions in isotropic turbulence conditions, droplet sizes in the inertial sub-range, and droplet breakup due solely by eddy-droplet collisions with smaller or the comparably-sized eddies is defined in terms of the droplet radius r as:

$$f(r) = K_b\, h(r)\, B_e.$$

K_b is a system dependent parameter that needs to be calibrated (see Zhao et al., 2014). The eddy-droplet collision frequency, h, is defined as:

$$h(r) = \int_{n_{e,m}} S_{ed}(u_e^2 + u_r^2)^{\frac{1}{2}} \overline{n}\, dn_e, \tag{45}$$

where $S_{ed} = \pi(r_e + r)^2$ is the collision cross-section area, r_e is the size of eddies which collide with a droplet of radius r, dn_e is number of eddies of size between r_e and $r_e + dr_e$. An estimate of the velocity square of the eddy is obtained from $u_e^2 = 3.8(\epsilon/k)^{\frac{2}{3}}$. Here ϵ is the kinetic energy dissipation rate, $k = \pi/r_e$ is wavenumber, and $u_r^2 = 1.7(\epsilon r)^{\frac{2}{3}}$ is the droplet velocity. The estimated number of eddies per unit volume of the fluid is found from $dn_{e,m}(k) = 3 \times 10^{-3} k^2 dk$ (see Azbel, 1981).

The breakup efficiency B_e is the probability of breakup if a drop-eddy collision takes place:

$$B_e = \exp\left[-\frac{E_c + E_v}{c_1 e}\right],$$

where E_c is the mean excess energy required for breakage into two equal-size drops and a small and a big daughter drop, and E_v is the (viscous and surface tension) energy associated with internal forces (see Zhao et al., 2014and Calabrese et al. (1986)). The minimum energy for droplet breakup is related to the amount of required energy to keep the surface of a droplet intact. In binary splitting,

$$E_c = 2\left[2\pi\sigma_d\left(\frac{r}{2^{1/3}}\right)^2 + \pi\sigma_d r_{\max}^2 + \pi\sigma_d r_{\min}^2 - 2\pi\sigma_d r^2\right]$$

where $e = \frac{1}{2}mu_e^2 = \frac{2}{3}\pi\rho_w r_e^3 u_e^2$, $r_{\min} = r_1$, $r_{\max} = r_m$, and σ_d is the droplet surface tension (see Zhao et al., 2014). The energy associated with internal forces is

$$E_v = \left[1 + a\exp\left(-\frac{T}{T_{tot}}\right)\right]\left[\frac{\pi}{6}\epsilon^{\frac{1}{3}}(2r)^{\frac{7}{3}}\mu_d\sqrt{\frac{\rho_w}{\rho}}\right], \tag{46}$$

where ρ_w is the fluid density, ρ is the density of the particular chemical complex oil density, T_{tot} is interaction simulation time (one time step of fluid-oil interaction), and μ_d is the oil species viscosity. The constant $a = 1.1$ is a calibration constant (see Zhao et al., 2014, Eq. (15)).

In Tsouris and Tavlarides (1994) it is argued that, assuming binary breakage (recall it was assumed that $\nu(V')$ is 2), the amount of energy required for the generation of two like-sized droplets is larger than what is required to produce one small and one big droplets. They suggested the breakup distribution of a drop of class size V, from a parent drop of class size V' is given by:

$$\beta(r, r') = \frac{E_{\min} + [E_{\max} - E(r)]}{\int_0^{r'}\{E_{\min} + [E_{\max} - E(r)]\}\, dr}, \tag{47}$$

where:

$$E(r) = 4\pi\sigma\left[(r'^3 - r^3)^{2/3} + r^2 - r'^2\right].$$

4.1.2. Parametrizing coalescence mechanics

The merging process in which two (or more) colliding droplets form a bigger droplet is called coalescence. The coalescence of droplets normally evolves in three stages: (1) collision; (2) interfacial drainage of liquid at touching interfaces; and (3) the rupture of the droplet surface. In this study we assume that background turbulence is the main cause for droplet collisions. The volume absorbed by a moving droplet when colliding with other droplets is the basis for calculating the collision frequency. The swept volume rate $h(V, V')$ is modeled following the kinetic gas theory. Assuming both droplets moving with turbulent eddies with relative velocity of c, a collision tube with cross section of $\pi(r + r')^2$ is swept. Therefore, the $h(V, V')$ could be defined as:

$$h(V, V'): = \pi(r + r')^2 c.$$

Assuming isotropic turbulence, it is reported in Kuboi et al. (1972) that the relative colliding velocity in stirred and pipe flows was well estimated as:

$$c^2 = 2\epsilon^{2/3}(r + r')^{2/3}.$$

In this work, uniform turbulence assumptions are used (see Kolmogorov, 1941). Assuming this is correct, the swept volume rate for droplets V and V' then reads:

$$h(V, V') = \frac{\pi}{4} 5.657\epsilon^{1/3}(r + r')^{7/3}.$$

The droplets need to stay in contact for a certain time to complete the coalescence process. Turbulence promotes collisions, however, it can also move the droplets away from each other before the coalescence process takes place. Therefore the collision efficiency is defined as the ratio between the average drainage time $\bar{t}$ and average contact time $\overline{\tau}$:

$$\lambda(V, V') = \exp\left\{-\frac{\bar{t}}{\overline{\tau}}\right\}.$$

See Prince and Blanch (1990). The drainage time of the thin interface between two droplets depends on the viscosities of each droplet and the main phase (could be different for air bubbles in comparison with oil droplets). As a result we need to be more careful about implementation of this parameter. The average drainage time for fully mobile interfaces is given by Prince and Blanch (1990), Eq. (18) :

$$\bar{t} = \left(\frac{R_{eq}^3 \rho_l}{16\sigma_d}\right)^{1/2} \ln\frac{h_0}{h_c},$$

where ρ_l is the density of the continuous phase, σ_d is the surface tension and h_0 is the initial film thickness. The critical film thickness h_c, as estimated in Chesters (1991), is

$$h_c = \left(\frac{A\, R_{eq}}{8\pi\sigma_d}\right),$$

where A is the Hamaker constant and R_{eq} is the equivalent droplet radius, given by:

$$R_{eq} = \frac{2}{1/r + 1/r'},$$

where r and r' are the radii of the colliding droplets. The average contact time $\overline{\tau}$ is given by (see Levich, 1962)

$$\overline{\tau} = 2^{2/3}\frac{(r + r')^{2/3}}{\epsilon^{1/3}}.$$

4.2. The complete depth-averaged model

We now summarize the physical/computational shallow-water oil fate model. In what follows, we will omit the chemical complex identifier of the droplet distribution. Consider a cell at position $\mathbf{x}$, and suppose that $s(\mathbf{x}, T)$, $C(\mathbf{x}, T)$ and $\overline{n}_j(\mathbf{x}, T)$, $j = 1, \cdots, m$ are known. We use the following split-step strategy to advance into $T + \Delta T$:

1. First the mass exchanges is computed with $s(\mathbf{x}, T)$ and (38) to obtain $s^* = s\left(\mathbf{x}, T + \frac{1}{2}\Delta T\right)$. For the subsurface, knowing $\overline{n}(\cdot, T')$ for $T' < T$, we produce the update $\overline{n}_j^*$ via (35) which includes the merging/splitting dynamics. The update for the submerged oil concentration C^* is computed by using $\overline{n}_j^*$ in (37).
2. To step to $T + \Delta T$, we use s^* and C^* to advance on (3) and (6) with $R = 0$ (it has already been taken into account in the half step).
3. Finally, the aggregated subsurface concentration $C(\mathbf{x}, T + \Delta T)$ is used to adjust the droplet distribution budget from the split-step as follows

$$\overline{n}_j(\mathbf{x}, T + \Delta T) = C(\mathbf{x}, T + \Delta T)\frac{\overline{n}_j^*}{C(\mathbf{x}, T + \frac{1}{2}\Delta T)}. \tag{48}$$

There is no expectation that droplets will retain their chemical complex composition over time and this issue is itself a very challenging modeling problem, well outside the scope of this study. Nevertheless, we can suggest how this challenge will be tackled: our goal is to deliver a chemical description of oil at the kilometer scales or greater and thus we will be upscaling the chemodynamics equations as well as applying dimension reduction strategies so that a smaller number of chemical complexes are tracked in space and time than the full complement of oil constituents. These chemical complexes are not expected to retain the dynamics of the oil constituents. Most critically, the chemical complexes will have memory terms that cannot be ignored. As reported and tested in Venkataramani et al. (2017), our dimension reduction strategy based upon embedding can capture memory effects over time scales closer to the macroscopic scales than the chemical scales. The depth-averaged algorithm presented above will need to be modified once chemodynamics are incorporated into the oil-fate model.

4.3. Computational complexity of the shallow-water oil fate model

Depth-averaging clearly produces computational efficiencies, when compared to the non depth-averaged case. It does so at the expense of loosing depth information of the oil. However, the oil fate model is being designed for use in shallow waters for the computation of oil spills over very large transverse scales and over significant time spans. It is thus suggested that a model with these characteristics will still be of great practical utility even if it is unable to resolve the vertical distribution of oil in these waters. In this study we develop a model that brings in critical oil dynamics that would be missed if all inherently vertically-distributed processes would be ignored in the oil-fate model, and these are mostly processes that bring their own challenge of coupling the micro and macroscales. We tackle directly the challenges posed by coupling of the microscale and macroscale by proposing a mass exchange model that upscales the microscale at the expense of fidelity. The use of upscaling and adiabatic assumptions in the mass exchange mechanics, proposed in this study, approximates critical microscale dynamics and balances without requiring resolving these. As a result, there is no significant increase in computational overhead.

To appreciate the computational efficiency of the oil fate model, we first compute the computational complexity of the oil model in three space dimensions and time and without making use of upscaling. We will also assume that the computations are explicit-in-time, since present codes are mostly designed that way to take advantage of shared/distributed memory computing machines. If the computation uses N_x spatial degrees of freedom and runs for N_T time steps, the computational complexity is $O([P \times N_x]^3 \times [Q \times N_T])$. The factor $P^3 \times Q$ represents the overhead multiplier if the microscale is to be resolved. In addition, we have a multiplicative factor of $O(I \times J)$, where I is the number of droplet size classes, and J is the number of chemicals. To appreciate the magnitude of the computational complexity, let us assume that the macroscale is to be resolved over kilometers, and the microscale to centimeters, P would be about 10^4 and Q would be comparable (an optimistic estimate) due to numerical stability constraints. The size classes I would be of order 10^1, J of order $10^2 - 10^3$. The complexity of the shallow-water oil model is $O(N_x^2 \times N_T)$, for the space/time discretization. The size classes I would be of order 10^1, J could be reduced to order of 10^1 if the dimension reduction strategy in Venkataramani et al. (2017) as applied to the chemodynamics equations delivers acceptable outcomes.

5. Results

We present three calculations. In Section 5.1 we focus on simulations that illustrate the complexity of the dynamics of buoyancy and wave breaking balances. The focus of the calculations in Section 5.2 will be on demonstrating, by comparison to data, that the considerably simpler birth/death model for droplet distribution dynamics proposed here is consistent with the more complex model of Tsouris and Tavlarides (Tsouris and Tavlarides, 1994). In Section 5.3 we incorporate the mass exchange mechanism developed here into a simplified version of the shallow-water oil transport model of Restrepo et al. (2015) to explore a nearshore oil pollution problem. The problem in question is called the *nearshore sticky water* conditions (see Restrepo et al., 2014).

In the calculations that follow we connote by *stack* a single vertical column of (the computational) domain of ocean. A stack is composed of a surface compartment, and a subsurface compartment, directly below. The surface compartment corresponds to the slick. The subsurface compartment has oil and water.

5.1. Mass exchanges in a single stack

Eqs. (35) and (38) were implemented on a single stack. The oil can only rise and sink within the stack and thus can only be present in the surface or sub-surface compartments. For this case the size classes were chosen using $r_1 = 25 \times 10^{-6}$ m and $r_m = 217 \times 10^{-6}$ m (25 and 317 μm, respectively). There were 17 different size classes. We simulated one hour of random wave breaking, with (14) setting $\lambda_b = \frac{1}{6T_w}$ (T_w being the wave period, see Restrepo et al., 2011), λ_b is the intensity parameter of the Poisson process. The wave amplitude was 1m. We initialized oil in the surface and in the subsurface boxes with equal volumes. Fig. 2 shows four cases, corresponding to different probability distributions for the breaking strength b_i. All cases show a very fast transient adjustment, followed by a slower evolution, largely dominated by buoyancy forces (for small b_i) and wave breaking (large b_i). In the large wave breaking regime the oil is mostly relegated to the subsurface. Clearly, the results differ from any steady-state concerning oil distributions on the surface and the subsurface.

A more detailed view of the overall distribution of the subsurface oil appears in Fig. 3. The distributions are plotted as 'equivalent thicknesses' of each size class, corresponding to the wave breaking strengths in Fig. 2. For small breaking strengths the small droplets stay in the subsurface and the larger ones buoyantly rise to the surface; the buoyancy forces are dominant. When the wave breaking strength is high the small droplets are affected dramatically in the subsurface as well as the larger droplets. The wave-breaking forces dominate.

The steady state assumption on droplet distributions depends very strongly on the distribution of droplets and on the strength of the breaking and, arguably, this assumption would be even more exceptional if transverse advection/dispersion affecting the oil droplet distribution in each stack is considered.

5.2. Benchmarking the merging and coalescence mechanics in our model

Our focus now turns to illustrating and benchmarking the birth/death droplet mechanics in our model. Specifically we compare our

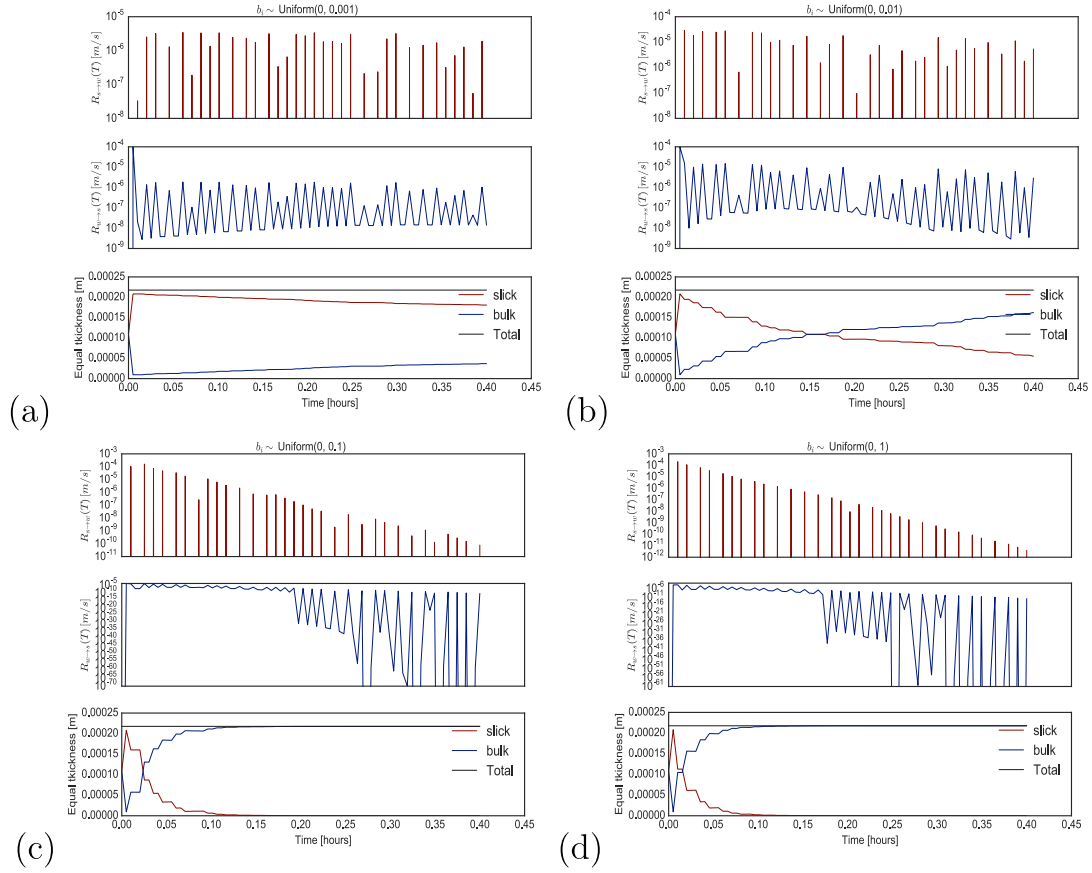

Fig. 2. Slick and subsurface oil mass exchanges expressed in terms of effective thickness (volume of oil per unit surface area of ocean) for a wave breaking strength of (a) $b_i \sim \text{Unif}(0, 10^{-3})$, (b) $b_i \sim \text{Unif}(0, 10^{-2})$, (c) $b_i \sim \text{Unif}(0, 10^{-1})$, (d) $b_i \sim \text{Unif}(0, 1)$. Unif is a random uniform distribution with a range specified by the argument in parenthesis. See Eqs. (35) and (38). For each group: top figure: rate of exchange from slick to subsurface $R_{s\to w}(T) = \sum_{i=1}^{N_b(T)} s(T_i) b_i \delta_{T_i}(T)$; middle figure: rate of exchange from subsurface to slick $R_{w\to s}(T) = \sum_{j=1}^{m} \frac{w_b(r_j)}{H} \overline{n}_j(T)$; bottom figure: total effective thickness of oil in the slick and subsurface, and their sum (which is shown to be conserved). Dynamics are given by (35) and (38). Wave amplitude is 1m, wave period is $T_w = 9.1$s, and the breaking rate is $1/6T_w$.

model results to experiments that track the cumulative volume fraction of a toluene and water mixture, as a function of droplet distribution and holdup conditions and time. The data is reported in Tsouris and Tavlarides (1994). In order to accomplish the comparison between our model and laboratory data we omit the slick dynamics, and suppress all of the mechanics in the subsurface dynamics, except for the terms associated with B_V and D_V in (39). The parameters for the model match those reported in connection with Figs. 3 and 4 in the Tsouris and Tavlarides paper: For continuous phase (water): the viscosity is $\mu_c = 1.787 \times 10^{-3}$ Ps, water density $\rho_w = 1025.0\,\text{kg/m}^3$, and the kinematic viscosity $\nu_c = \mu_c/\rho_w\ \text{m}^2/\text{s}$. For the dispersed phase (toluene), we chose a surface tension $\sigma_d = 28.4 \times 10^{-3}$ N/m, a dispersed phase molecular viscosity $\mu_d = 0.59 \times 10^{-3}$ Ps , and a density $\rho = 865\ \text{kg/m}^3$. The droplets ranged in size from $r_1 = 100 \times 10^{-6}$ m to $r_m = 380 \times 10^{-6}$ m (100 and 380 μm, respectively), and we used 25 droplet size classes ($m - 1 = 25$). In Fig. 4 we superimpose the output of our model (lines) with dots representing the experimental data in Tsouris and Tavlarides (1994) (originally obtained by Bae and Tavlarides, 1989). Our results show consistency between our simpler model and data, and by implication, consistency with the more complex model proposed by Tsouris and Tavlarides (1994). The numerical results suggest that the simplifications we made primarily affect the fidelity of the dynamics of the larger droplet size classes. The degradation is an acceptable tradeoff with gains in computational efficiency.

5.3. Mass exchanges in the nearshore sticky waters problem

An explanation for the slowing down of shoreward-directed buoyant pollutant transport in proximity of the shore was proposed in Restrepo et al. (2014). The mechanism can be summarized as follows: the transport of buoyant pollutants toward the shore, by the action of ocean currents and the residual flow due to waves, proceeds nearly ballistically when the pollutant occupies the thinnest possible region of the water column, close to the surface. However, the transport can slow down significantly, due to increased entrainment and friction if the pollutant distributes itself widely within the water column. The effect is particularly strong when there is a great deal of mixing or the bathymetry is shallow and/or rough. In fact, the depth-averaged transport has an effective advection that can go to zero under certain circumstances, away from the shore. In such case the average transport of pollutant can slow down and park the pollutant some distance away from the shore. If any of the pollutant reaches the beach it does so primarily by diffusion.

Since the vertical distribution of the oil plays a critical role, we revisit the simple conceptual model used in Restrepo et al. (2014) and updated in Restrepo et al. (2015), replacing the simple mass exchange model used in these with the entrainment model proposed in this work. The basic scenario is presented in Section 6.1 of Restrepo et al. (2015). The domain for the computation is shown schematically as Fig. 5 in Restrepo et al. (2015). The changes to the original model, given by Eqs. (39), (40), and (43) in Restrepo et al. (2015), and the one captured by

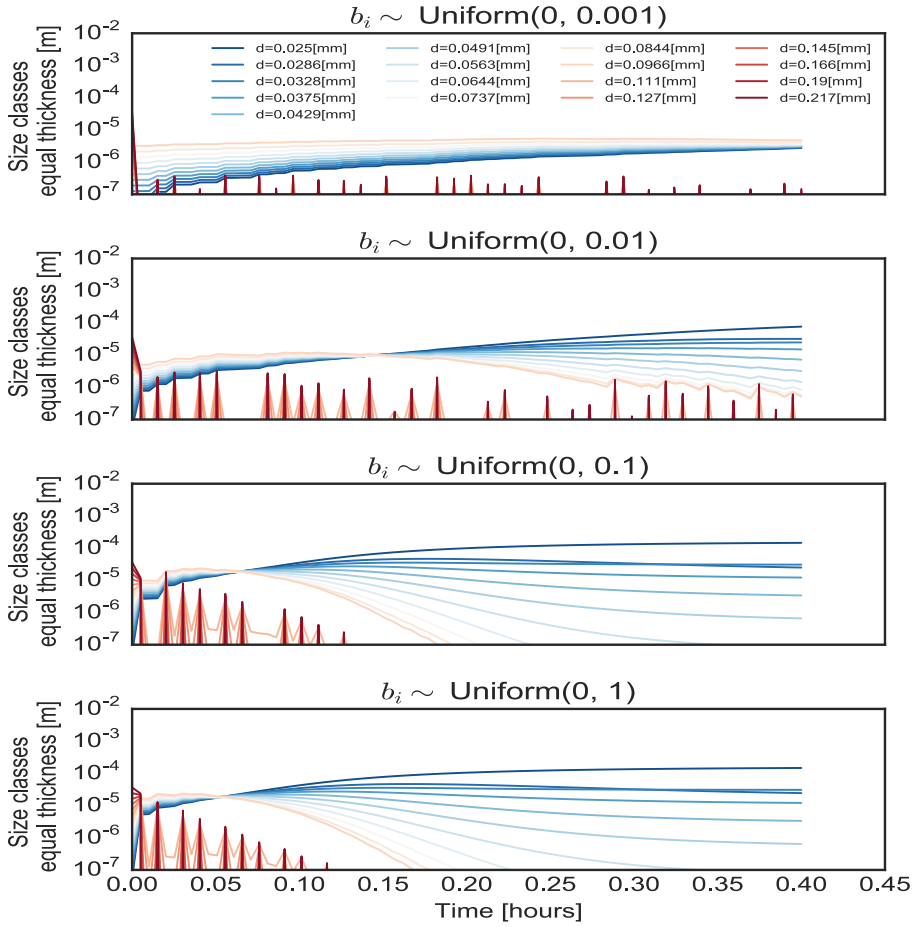

Fig. 3. Subsurface oil size distributions as a function of time for different wave breaking strengths, giving more detail on the total oil balances shown in Fig. 2. Dynamics are given by (35) and (38). Wave amplitude is 1m, wave period is T_w = 9.1s, and the breaking rate is $1/6T_w$.

(3), (6) and (18), in the algorithmic process described in Section 4.2, are as follows:

- The subsurface oil will be captured by 4 size classes, chosen in the range $r_1 = 100 \times 10^{-6}$m and $r_m = 380 \times 10^{-6}$m (a range of droplets suggested by North et al., 2015).
- For simplicity, we will employ a constant mixed layer depth P in the calculations. (In Restrepo et al., 2015 P is a function of position x).
- In Restrepo et al. (2014) the mass exchange term in the dynamics of the slick and the subsurface oil used in the original model reads $\frac{(1-\gamma)s-\gamma P(x)S}{\varsigma(x)}$), where γ is a constant fraction parameter that regulates the rate of exchange of surface and subsurface oil, ς is the relaxation rate parameter, the oil in the surface is s and in the subsurface it is $P(x)S$.
- The mass exchange component of the subsurface associated with oil entrainment due to wave breaking $s(T)b(T)$ in (18) is complemented by $s(T)\frac{2\epsilon}{\rho_w g A^2}$. Here, ϵ is the wave action damping (see Equation (33) of Restrepo et al. (2015)), ρ_w is the ocean density, g is gravity, and A is the wave amplitude. In the calculations that follow, the wave amplitude in the deeper end of the domain is 1 m, and the wave period is 9.1 s. The driving velocity is solely due to wave generated transport, or Stokes drift (see McWilliams and Restrepo, 1999). The new term accounts for the intense turbulence associated with the shoaling process of the waves. In general it tends to dominate the mass exchanges due to wave breaking in the shoaling region.

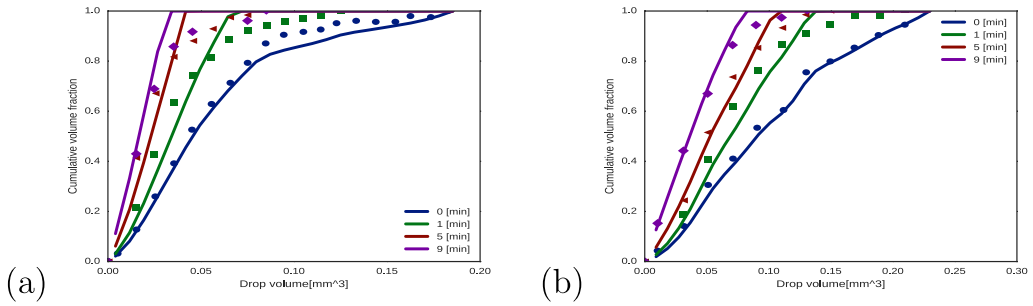

Fig. 4. Comparison of the time evolution of the cumulative droplet distribution $\int_{V_1}^{V} \overline{n}(V', T)dV'$ of data and of predictions by Eq. (39). Experimental data was taken from Tsouris and Tavlarides (1994) and reported originally in Bae and Tavlarides (1989). Comparison of our model results with Figs. 3 and 4 of Tsouris and Tavlarides (1994). (a) Corresponds to a (holdup) ratio of oil-to-water of 0.1; (b) corresponds to an oil-to-water ratio of 0.2.

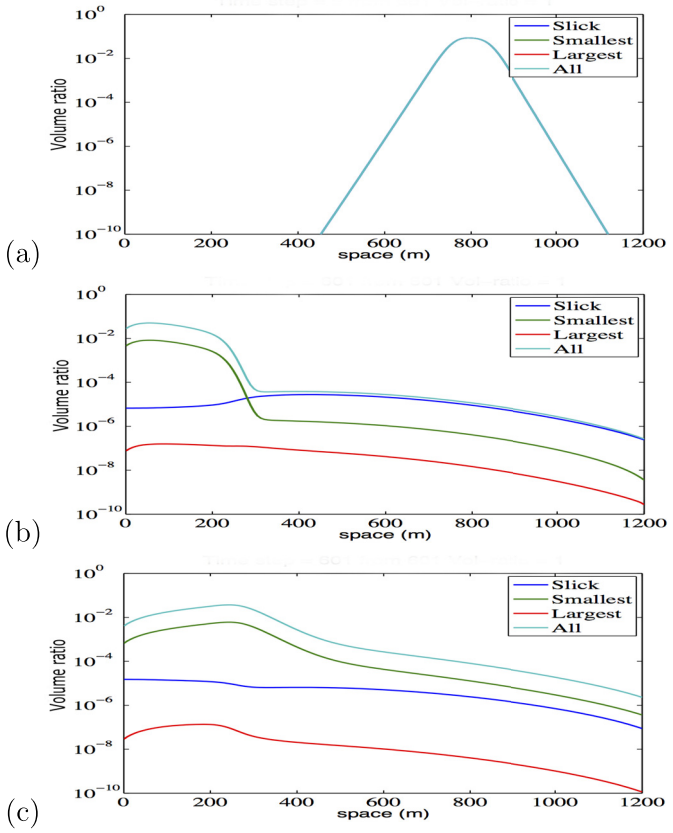

Fig. 5. Slick and subsurface oil. Initially (a), and after roughly 100 h, (b) and (c). All of the oil is initially in the slick. The total oil initially and throughout the calculation is $\text{vol}_{tot} = 2.334 \times 10^{-3}$ m$^3/m^2$, constant; (b) corresponds to the oil distribution at the final time, with a mixed layer thickness of $P = 1$m, and (c) corresponds to the oil distribution at the final time for a mixed layer thickness $P = 6$m. When the thickness of the mixed layer is large the center of mass of the oil shifts away from the shore. Note that the vertical axis, corresponding to the ratio of oil in the size class or in the slick to vol_{tot}, is logarithmic. The labels 'all', 'smallest' and 'largest' refer to the total subsurface oil, the smallest and the largest class sizes in the subsurface oil in the calculations.

Each computational grid location in the transverse coordinate x has a stack composed of a multi-size subsurface compartment, and an upper slick compartment. The x coordinate refers to the distance from the shore (alongshore are ignored). The specifics of the calculation are as follows: at time T, the stack balance of oil is updated after the transverse distribution of oil is advected/dispersed (this is an adiabatic approximation that is based on the disparate time scales in which oil in the vertical direction rebalances, compared with the slower times of transverse advection). The imposed transport velocity is approximately 0.02 m/s and is consistent with the transport imparted by the Stokes drift velocity due to gravity waves of about 1m height and 9.1 s periods. The mass exchange within each stack is run for about 1.5 h of simulated time. Then the advection and dispersion across the coupled stacks is performed. This process is repeated. The total simulated time is 100 hrs. The parameters used in the calculation are the same as those that were used to generate Fig. 7 of Restrepo et al. (2015). Fig. 5a shows the initial oil distribution. The total amount of oil is constant over time and equal to $\text{vol}_{tot} = 2.334 \times 10^{-3}$ m$^3/m^2$. All of the oil is initially in the slick. Fig. 5b and c show the final oil distribution. The oil is reported on a logarithmic scale as the volume ratio with respect to v_{tot} in each size class or in the slick. The cases shown in Fig. 5b and c differ only in the thickness of the mixed layer, with (b) corresponding to $P = 1$m, and (c) to $P = 6$m. As was shown in Restrepo et al. (2014) and Restrepo et al. (2015) the $P = 1$m case shows little evidence of slowing or parking. In the earlier papers we reported that the oil that initially started in the slick stayed in the slick even very close to the shore. This is no longer the case with the mass exchange term proposed in this paper: After 100 h of simulated time the slick still accounts for most of the oil away from the shore, but there is a redistribution of the oil between the slick and the subsurface due to shoaling. Moreover, the bulk of the subsurface oil is found in the smaller droplet size class. After 100 h of simulated time, the $P = 6$ m case leads to results that do not differ from the results with the old mass exchange term, however, there is a more complicated distribution. Namely, for this case, oil parks away from the shore. The center of mass is roughly 200m away from the shore. The oil has also redistributed between the slick and the subsurface both close as well as far away from the coast. In this case we also find that the subsurface oil has a larger concentration of small droplet sizes.

6. Summary

In Restrepo et al. (2015) an Eulerian oil fate model was proposed. The model is specialized to shallow waters and is being designed to approximate the oil dynamics at environmental spatio-temporal scales: from hundreds of seconds to seasons, and hundreds of meters to hundreds of kilometers. It is a depth-averaged transport model that includes advection and dispersion due to wind, waves, and currents, and captures the dynamics of oil in terms of two compartments: a surface compartment, or 'oil slick', and a subsurface compartment. The oil slick is thus the portion of the oil in proximity of, or at the sea surface itself. The subsurface oil is the remaining portion, distributed throughout the water column, in the form of droplets with a dispersive distribution. In order to provide an accounting of the chemical composition of the oil spill a future version of the model will include chemodynamics. Chemodynamics will also have a bearing on the transport dynamics of oil, since chemistry affects the macroscopic realm (*e.g.*, photolysis, sedimentation, evaporation, etc) as well as the microscopic, via changes in the surface tension and viscosity of the oil droplets.

The present study focused on the development of a model for the mass exchanges between the surface and subsurface oil. The model takes into account the entrainment/mixing caused by sea surface intermittencies (e.g. white-capping, see Restrepo et al., 2011), the merging and splitting of droplets, and oil droplet buoyancy/drag effects. The starting point of the mass exchange model proposed here is found in Tkalich and Chan (2002). Aside from upscaling and depth-averaging the most salient difference between their model and ours is that the model proposed here does not assume time stationarity or equilibration. We also work out in detail the momentum balances of buoyancy and near-surface mixing and how these affect the dynamics of droplet merging/splitting and their vertical distribution. The droplet distribution dynamics model we adopted/modified is largely inspired by the work of Tsouris and Tavlarides (1994). We tested the proposed upscaled droplet distribution dynamics against data, with good outcomes.

The model takes into account microscopic dynamics without resolving them. At the heart of the upscaling strategy is the use of an adiabatic approximation, that assumes that the dynamics of the droplets settle at time scales much shorter than the macroscopic time scales of the transverse advection/dispersion of oil, and depth-averaging and filtering and stochastic parametrization. Depth-averaging is justified in oceanic regions where barotropic flows have small aspect ratios. These conditions can be found in the shallow reaches of the continental shelf and the nearshore. The upscaling strategies lead to a practically-implementable model at the expense of fidelity. We provided estimates of efficiency in our approach and suggest that these make the Eulerian framework of the oil model we are developing practical and its computer implementation, feasible.

We also took the opportunity in this study to apply the mass exchange model developed here on a geophysical problem related to buoyant pollutant transport in the nearshore. The specific problem considered is *nearshore sticky waters*, detailed in Restrepo et al. (2014).

Nearshore sticky waters refers to oceanic conditions that lead to the slowing down and possibly parking of shoreward-propagating buoyant tracers. The thickness of the vertical mixing layer, when compared to the overall water column depth turns out to be critical for sticky conditions. In this study we replace the original fixed mixed layer depth by the time dependent and oil droplet distribution dependent layer produced by the mass exchange model developed in this study. Doing so still lead to situations whereby nearshore sticky waters were possible. Further, the addition of the mass exchange mechanism demonstrates that mixing, the type of oil and the droplet distribution dynamics will influence oil budgets and the manner in which oil distributes itself vertically under nearshore sticky water conditions.

Most ocean oil fate models are Lagrangian. The mass exchange model developed here is intended to be retrofitted into an Eulerian framework. The specific oil fate model is in Restrepo et al. (2015), however, the mass exchange dynamic proposed here can, in principle, be included in any other Eulerian model.

Acknowledgments

This work was supported by GoMRI and by NSF DMS grants 1524241, 1434198 and 1109856. JMR also acknowledges the hospitality of Stockholm University, where some of this work was done, and the support provided by a Stockholm University Rossby Fellowship. JMR also thanks the Kavli Institute of Theoretical Physics, at the University of California, Santa Barbara where some of this research was done. The KITP is supported in part by the National Science Foundation under Grant No. NSF PHY-1748958. SV acknowledges the support from the Simons Foundation through a collaboration grant award 524875.

References

Aman, Z.M., Paris, C.B., May, E.F., Johns, M.L., Lindo-Atichati, D., 2015. High-pressure visual experimental studies of oil-in-water dispersion droplet size. Chem. Eng. Sci. 127, 392–400.

ASCE Task Committee on Modeling of Oil Spills of the Water Resources Engineering Division, 1996. State of the art review of modeling transport and fate of oil spills. J. Hydraul. Eng. 122, 594–609.

Azbel, D., 1981. Two-Phase Flows in Chemical Engineering. Cambridge University Press.

Azevedo, A., Oliveira, A., Fortunato, A.B., Zhang, J., Baptista, A.M., 2014. A cross-scale numerical modeling system for management support of oil spill accidents. Mar. Pollut. Bull. 80, 132–147.

Bae, J., Tavlarides, L.L., 1989. Laser capillary spectrophotometry for drop-size concentration measurements. Am. Instit. Chem. Eng. J. 35, 1073.

Belore, R., Trudel, K., Mullin, J., Guarino, A., 2009. Large-scale cold water dispersant effectiveness experiments with alaskan crude oils and corexit 9500 and 9527 dispersants. Mar. Pollut. Bull. 58, 118–128.

Calabrese, R.V., Chang, T.P.K., Dang, P.T., 1986. Drop breakup in turbulent stirred-tank contactors. part i: effect of dispersed-phase viscosity. Am. Insti. Chem. Eng. J. 32 (4), 657–666.

Chen, Z., 2007. Reservoir Simulation: mathematical Techniques in Oil Recovery. Vol. 77 SIAM CBMS-NSF Regional Conference Series in Applied Mathematics.

Chesters, A.K., 1991. The modelling of coalescence processes in fluid-liquid dispersions: a review of current understanding. Chem. Eng. Res. Des. 69 (A4), 259–270.

Daling, P., Leirvik, F., Almas, I., Brandvik, P.J., Hansen, B.H., Lewis, A., Reed, M., 2014. Surface weathering dispersivity. Mar. Pollut. Bull. 87, 300–310.

Daling, P., Strom, T., 1999. Weathering of oils at sea: model/field data comparisons. Spill Sci. Technol. Bull. 5, 63–74.

Delvigne, G., Sweeney, C.E., 1988. Natural dispersion of oil. Oil Chem. Pollut. 4, 281–310.

Dominicis, M.D., Pinardi, N., Zodiatis, G., Archetti, R., 2013. MEDSLIK-II, A lagrangian marine surface oil spill model for short-term forecasting - part 2: numerical simulations and validations. Geosci. Model Dev. 6, 1871–1888. https://doi.org/10.5194/gmd-6-1871-2013.

Hammam, S.E.M., Hamoda, M.F., Shaban, H.I., Kilani, A.S., 1988. Crude oil dissolution in saline water. Water Air Soil Pollut. 37, 55–64.

Kolmogorov, A.N., 1941. Local structure of turbulence in incompressible viscous fluid of very large reynolds number. Doklady Akademiya Nauk SSSR 30, 299–301.

Kuboi, R., Komasawa, I., Otake, T., 1972. Behavior of dispersed particles in turbulent liquid flow. J. Chem. Eng. Jpn. 5 (4), 349–355.

Lehr, W., Jones, R., Evans, M., Simecek-Beatty, D., Overstreet, R., 2002. Revisions of the ADIOS oil spill model. Environ. Model. Softw. 17, 191–199.

Lehr, W., Overstreet, R., Jones, R., Watabayashi, G., 1992. ADIOS-Automated Data Inquiry for Oil Spills. EC/EPS–93-01710, Canada.

Lehr, W.J., 2001. Review of modeling procedures for oil spill weathering behavior. In: Brebbia, C.A. (Ed.), Advances in Ecological Models. WIT Press, pp. Chapter3.

Levich, V.G., 1962. Physicochemical Hydrodynamics. Prentice-Hall, Englewood Cliffs, NJ.

Li, Z., 2009. Wave tank studies on chemical dispersant effectiveness: dispersed oil droplet size distribution. Environ. Eng. Sci. 9, 1407–1418.

Liao, Y., Lucas, D., 2009. A literature review of theoretical models for drop and bubble breakup in turbulent dispersions. Chem. Eng. Sci. 64 (15), 3389–3406.

Loebing, C., 2015. Sinking of crude oil amended-model oil mixtures due to evaporative or dissolution weathering on the surface and submerged in water.

Loh, A., Shim, W.J., Ha, S.Y., Un, H., 2014. Oil-suspended particulate matter aggregates: formation mechanism and fate in the marine environment. Ocean Sci. J. 49, 329–341.

Lonin, S.A., 1999. Lagrangian model for oil spill diffusion at sea. Spill Sci. Technol. Bull. 5, 331–336.

Maas, U., Pope, S.B., 1992. Chemical kinetics: intrinsic low-dimensional manifolds in combustion space. Combust. Flame 88, 239–264.

McWilliams, J.C., Restrepo, J.M., 1999. The wave-driven ocean circulation. J. Phys. Oceanogr. 29, 2523–2540.

McWilliams, J.C., Restrepo, J.M., Lane, E.M., 2004. An asymptotic theory for the interaction of waves and currents in coastal waters. J. Fluid Mech. 511, 135–178.

McWilliams, J.C., Sullivan, P.P., Moeng, C.-H., 1997. Langmuir turbulence in the ocean. J. Fluid Mech. 334, 1–30.

Mitzenmacher, M., 2003. A brief history of generative models for power law and lognormal distributions. Internet Math. 1, 226–251.

North, E.W., Adams, E.E., Thessen, A.E., Schlag, Z., He, R., Socolofsky, S.A., Masutani, S.M., Peckham, S.D., 2015. The influence of droplet size and biodegradation on the transport of subsurface oil droplets during the deepwater horizon spill: a model sensitivity study. Environ. Res. Lett. 10, 024016.

Prince, M., Blanch, H.W., 1990. Bubble coalescence and break-up in air-sparged bubble columns. Am. Instit. Chem. Eng. J. 36 (10), 1485–1499.

Reed, M., Johansen, O., Leirvik, F., Brors, B., 2009. Numerical algorithm to compute the effects of breaking waves on surface oil spilled at sea. final report submitted to. vol 19.

Restrepo, J.M., Ramírez, J., Venkataramani, S., 2015. An oil fate model for shallow-waters. J. Mar. Sci. Eng. 3, 1504–1543.

Restrepo, J.M., Ramírez, J.M., McWilliams, J.C., Banner, M., 2011. Multiscale momentum flux and diffusion due to whitecapping in wavecurrent interactions. J. Phys. Oceanogr. 41, 837–856.

Restrepo, J.M., Venkataramani, S.C., Dawson, C., 2014. Nearshore sticky waters. Ocean Modell. 80, 49–58.

Romero, L., Siegel, D., McWilliams, J., Uchiyama, Y., Jones, C., 2016. Characterizing stormwater dispersion and dilution from small coastal streams. J. Geophys. Res. Oceans 121, 3926–3943.

Romero, L.E., Uchiyama, Y., Siegel, D., McWilliams, J., Ohlmann, C., 2013. Simulations of particle-pair dispersion in southern california. J. Phys. Oceanogr. 43, 1862–1879.

Sokolofsky, S., Adams, E.E., Sherwood, C.R., 2011. Formation dynamics of subsurface hydrocarbon intrusions following the deepwater horizon blowout. Geophys. Res. Lett. 88. https://doi.org/10.1029/2011GL047174.

Thibodeaux, L.J., 1996. Environmental Chemodynamics. John Wiley.

Tkalich, P., Chan, E.S., 2002. Vertical mixing of oil droplets by breaking waves. Marine Pollut. Bull. 44, 1219–1229.

Tkalich, P., Chan, E.S., 2006. A CFD solution of oil spill problems. Environ. Modell. Software 21, 271–282.

Transportation Research Board and National Research Council, 2003. Oil in the Sea III: Inputs, Fates, and Effects. The National Academies Press, Washington, DC. https://doi.org/10.17226/10388.

Tsouris, C., Tavlarides, L.L., 1994. Breakage and coalescence models for drops in turbulent dispersions. Am. Instit. Chem. Eng. J. 40 (3), 395–406.

Uchiyama, Y., Idica, E., McWilliams, J., Stolzenbach, K., 2014. Wastewater effluent dispersal in two southern california bays. Cont. Shelf Res. 76, 36–52.

Venkataramani, S., Venkataramani, R., Restrepo, J.M., 2017. Dimension reduction for systems with slow relaxation. J. Stast. Phys. 167, 892–933. https://doi.org/10.1007/s10955-017-1761-7.

Wang, J., Shen, Y., 2010. Modeling oil spills transportation in seas based on unstructured grid, finite-volume, wave-ocean model. Ocean Modell. 35, 332–344.

Yapa, P., Zheng, L., Nakata, K., 1999. Modeling underwater oil/gas jets and plumes. J. Hydraul. Eng. 125, 481–491.

Zelenke, B., O'Connor, C., Barker, C., Beegle-Krause, C., Eclipse, L., 2012. .

Zhao, L., Torlapati, J., Boufadel, M., King, T., Robinson, B., Lee, K., 2014. VDROP: A comprehensive model for droplet formation of oils and gases in liquids–incorporation of the interfacial tension and droplet viscosity. Chem. Eng. J. 253, 93–106.